STRUCTURAL ANALYSIS OF FLOATING PIPES OF THE FISH CAGE IN CURRENTS

XIAODONG BAI*, YUNPENG ZHAO AND GUOHAI DONG

State Key Laboratory of Coastal and Offshore Engineering, Dalian University of Technology, Dalian 116024, China.
* Corresponding author. E-mail: zzubxd@163.com

Key words: Structural analysis, floating pipes, finite element method, hydrodynamic model

Abstract. A numerical model is developed to investigate the structural performance and stress distribution of floating pipes of fish cage subjected to the flow. The modeling approach is based on the joint use of the finite element method using the shell elements to simulate the floating pipes and the hydrodynamic force model improved from the Morison's equation and lumped-mass method. The hydrodynamic response of the fish cage and forces on the floating pipes can be obtained by the Morison's equation and lumped-mass method. The stress and deformation of the floating pipes can be evaluated using the finite element method. Using an appropriate iterative scheme, the stress distribution and maximum stress of the floating pipes can be obtained using the proposed model. To validate the numerical model, the numerical results were compared with the data obtained from corresponding physical model tests. The comparisons show the numerical results agree well with the experimental data. On that basis, the simulations of floating pipes in currents are performed to investigate the maximum stress and the critical locations. Simulations of the fish cage in different flow velocity are performed. The effect of the velocity on the deformations and stress of the floating pipes is analyzed. The simulations results show that the stress and deformations drastically increases with the increase of flow velocity. Comparing results of floating pipes with different mooring line arrangements indicates that increasing mooring lines can efficiently lower the stress of the floating pipes. The simulation of the SPM cage system with multiple net cages in current is preformed and the results show the middle cage is most dangerous for the tripartite-cage system.

1 INTRODUCTION

As the fish cage is located in the unprotected open ocean and exposed to the rigorous environment condition, understanding the hydrodynamic characteristics of fish cages and ensuring the reliability and security of marine cage are becoming a crucial issue.

Numerous studies previously have been performed focusing mainly on the hydrodynamic characteristics of net cages. Tsukrov et al.[1] proposed a consistent finite element to model the hydrodynamic response of net panels and applied to evaluate the performance of a tension leg fish cage in the open ocean environment. Lader and Enerhaug[2] conducted a series of experiments and developed computational models to investigate the force and deformation on a net cage exposed in uniform flow. Moe et al.[3] analyzed the deformation of a net cage in currents of different velocities utilizing commercial explicit finite element software ABAQUS and demonstrated that the numerical results was significantly consistent with that of

experiment. Kristiansen and Faltinsen[4] proposed a screen type force model for the viscous hydrodynamic load on nets and simulated the net by a system of trusses and investigated the mooring load on the net cage by experimental and numerical study. Zhao et al.[5] analysed the deformations of the floating collar in waves using curved beam method.

Because of its economic benefits and corrosion resistance, the high-density polyethylene (HDPE) floating pipes have been widely used in constructing the floating system of fish cage. However, the application of HDPE pipe increases the risk of the failure because the composite has relatively low strength. To improve the understanding of the structural performance and stress distribution of the floating system, a numerical model is presented in current study.

The paper is organized as follows. Section 2 describes the finite element method, the lump-mass model and the joint use of the two numerical models. In Section 3, the finite element model and the lump-mass model are validated against corresponding physical model tests. Section 4 presents the numerical simulations of the fish cage at different flow velocity and analyses the effect of the mooring line arrangements and simulates the single point mooring (SPM) cage system with multiple net cages in current. Finally, in Section 5, conclusions are presented.

2 DESCRIPTION OF THE NUMERICAL MODEL

2.1 Model of the floating pipe

2.1.1 Finite element model

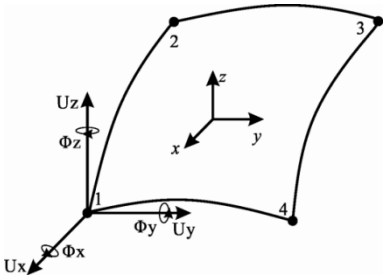

Fig. 1. The four-node shell element.

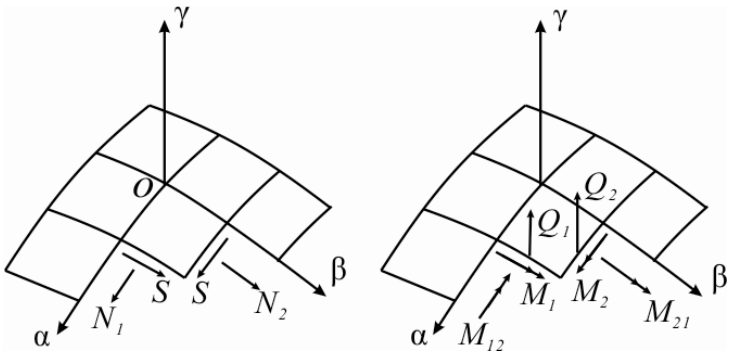

Fig. 2. The free-body diagram of the shell element.

The floating system of the net cage is constructed with HDPE pipes in most marine fish producing countries. To understanding the structural performance, the finite element model of the floating pipes was performed using shell elements. The applied element is suitable for analyzing thin to moderately-thick shell structures, which is a four-node element with six degrees of freedom at each node: translations in the *x, y,* and *z* directions and rotations about the *x, y,* and *z*-axes, as shown in Fig. 1.

Fig. 2 shows the free-body diagram of the shell element. According to the Kirchhoff-Love hypotheses, the equilibrium equations relationship are obtained as following:

$$\begin{cases} \dfrac{\partial}{\partial\alpha}(BN_1)-\dfrac{\partial B}{\partial\alpha}N_2+\dfrac{\partial A}{\partial\beta}S+\dfrac{\partial}{\partial\beta}(AS)+ABk_1Q_1+ABX=0 \\ \dfrac{\partial}{\partial\beta}(AN_2)-\dfrac{\partial A}{\partial\beta}N_1+\dfrac{\partial B}{\partial\alpha}S+\dfrac{\partial}{\partial\alpha}(AS)+ABk_2Q_2+ABY=0 \\ -AB(k_1N_1+k_2N_2)+\dfrac{\partial}{\partial\alpha}(BQ_1)+\dfrac{\partial}{\partial\beta}(AQ_2)+ABZ=0 \\ \dfrac{\partial}{\partial\alpha}(BM_{12})-\dfrac{\partial B}{\partial\alpha}M_{12}+\dfrac{\partial A}{\partial\beta}M_1+\dfrac{\partial}{\partial\beta}(AM_2)-ABQ_2=0 \\ \dfrac{\partial}{\partial\beta}(AM_{12})-\dfrac{\partial A}{\partial\beta}M_{12}+\dfrac{\partial B}{\partial\alpha}M_2+\dfrac{\partial}{\partial\alpha}(BM_1)-ABQ_1=0 \end{cases} \tag{1}$$

where *u, v, w* are the displacements in the coordinate*α-β-γ*. *A, B* is Lame coefficient; N_1, N_2, S, Q_1, Q_2 and M_1, M_2, M_{12}, M_{21} are the film internal forces and bending moments, respectively. *X, Y, Z* are external forces along the three principal axes. The external loads on the floating pipes can be determined using a modified Morison's equation, which are presented in the section 2.1.2.

2.1.2 Hydrodynamic response of the floating pipes

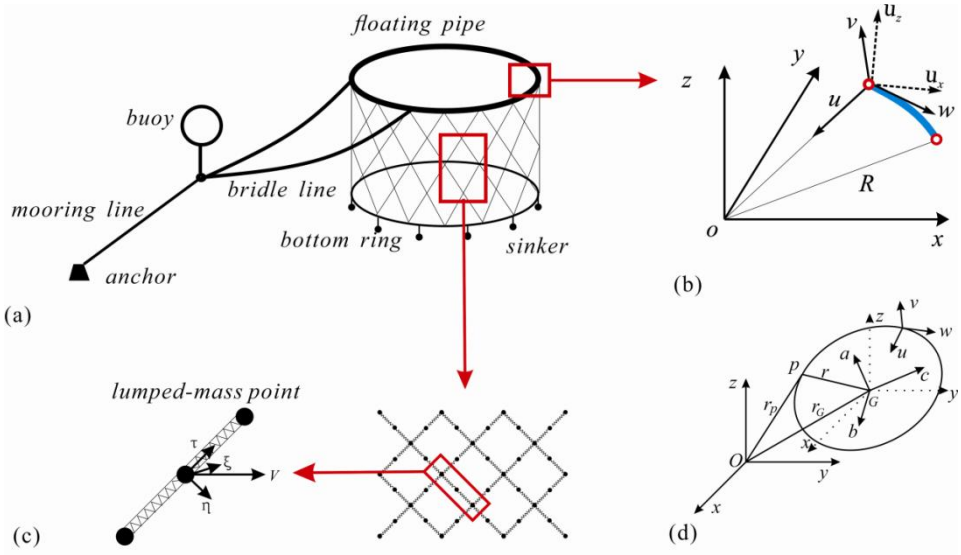

Fig. 3. The lumped-mass model of the net cage: (a) schematic diagram of a single-point mooring cage system; (b) a sketch of the floating pipe mini-segment; (c) schematic diagram of mass-spring model for net; (d) schematic diagram of moving coordinates system.

The floating system of a fish cage is at the free water surface and the floating pipes bears the most wave-induced loads. It is assumed that the floating system will have no influence on waves because its size is much smaller than the wavelength. When calculating wave force, the floating pipes are divided into many mini-segments as shown in Fig. 3(b). The wave forces on the float pipes can be evaluated from Morison's formula. In this paper, the form of Morison's formula given by Brebbia and Walker[6] is employed, which is shown as follows:

$$F = \frac{1}{2} C_D \rho A |\vec{u} - \vec{U}| \cdot (\vec{u} - \vec{U}) + \rho V_0 \vec{a} + C_m \rho V_0 (\vec{a} - \vec{U}) \quad (2)$$

where $\vec{u}$ and $\vec{U}$ are the velocity vectors of water particles and the mini-segment, respectively; $\vec{a}$ and $\vec{U}$ are the acceleration vectors of water particles and the mini-segment, respectively; ρ is the water density; V_0 is the underwater volume of the mini-segment; A is the projected area normal to the wave-propagation direction; C_D and C_m are the drag and added mass coefficients.

To obtain the motions of the floating collar, coordinate systems are defined: the global coordinate system *x-y-z*, the body-coordinate system *a-b-c*, and the local coordinate system *u-w-v* as shown in Fig. 3(d). Initially, axes *x, y* and *z* are parallel to axes *a, b* and *c,* respectively. According to Newton's second law and the Euler equations of motion, six equations of motion are shown as follow:

$$\begin{aligned} &\ddot{x}_G = \frac{1}{m_G}\sum_{j=1}^{n} F_{x_j}, \qquad \ddot{y}_G = \frac{1}{m_G}\sum_{j=1}^{n} F_{y_j}, \qquad \ddot{z}_G = \frac{1}{m_G}\sum_{j=1}^{n} F_{z_j} \\ &I_a \frac{\partial \omega_a}{\partial t} + (I_c - I_b)\omega_c \omega_b = M_a, \quad I_b \frac{\partial \omega_b}{\partial t} + (I_a - I_c)\omega_a \omega_c = M_b, I_c \frac{\partial \omega_c}{\partial t} + (I_b - I_a)\omega_a \omega_b = M_c \end{aligned} \quad (3)$$

where $F_{x_j}, F_{y_j}, F_{z_j}$ are the components of the force vector. F_j (j=1,n) along global coordinate axes *x-y-z, n* is the number of external forces, and m_G is the mass of the rigid body; $\ddot{x}_G$, $\ddot{y}_G, \ddot{z}_G$ are accelerations of the collar rigid centroid. The subscripts *a*, *b*, and *c* represent the body-coordinate axes *a*, *b*, and *c*; M_a, M_b and M_c (j=1,n) are the components of the moment vector M_j (j=1,n) along the principal axes; I_a, I_b, I_c are the components of the moments of inertia *I* along the three moving coordinate axes; ω_a, ω_b, ω_c are the angles of rotation along the three moving coordinate axes.

2.2 Model of the flexible net

As the net is attached to the floating pipes, the floating pipes are subjected to not only the wave forces but also the net tensions. The net forces on floating pipes play an important role in the dynamic response of the floating pipes. The net forces can be determined by dynamical simulation which is based on the lumped-mass method. The net is simulated as a series of lumped mass points that are connected with springs as shown in Fig. 3(c). Based on the link relationship, the external force acting on each element is calculated and distributed to the corresponding lumped mass point.

According to Newton's second law, the motion equation of a lumped mass i in waves can be expressed by

$$M_i a = \sum_{j=1}^{n} T_{ij} + F_D + F_I + W + B \quad (4)$$

where, *a* is the acceleration of mass point i, T_{ij} is the vector of the tension in bar *ij* (*j* is the code for knots at another end of bar *ij*), *n* is the numbers of adjacent knots of point *i*, F_D is the drag force, F_I is the inertial force, *W* is the gravity force, *B* is the buoyancy force.

To calculate the hydrodynamic forces acting on the net cage and mooring system, the entire cage system is divided into many structural elements that are subjected to wave loadings, as shown in Fig. 3(c). To simplify numerical simulations, each element is treated as a small body since the element size is relatively small comparing to the characteristic wavelength. Thus, it is appropriate to apply the modified Morison equation including the

relative motion between the structural element and the surrounding fluid, The τ component of the drag force of point i can be represented by

$$F_{d\tau} = -\frac{1}{2}\rho C_{d\tau} Dl\left|\dot{\tau} - e_\tau \cdot V\right|\left(\dot{\tau} - e_\tau \cdot V\right) \tag{5}$$

where $C_{d\tau}$ represent the drag coefficient of the τ component, D cylindrical element diameter, l cylindrical element length. The τ, η and ξ components of the relative velocity of point i are $\dot{\tau} - e_\tau \cdot V$, $\dot{\eta} - e_\eta \cdot V$ and ξ, respectively. The same expression can be applied for other drag forces ($F_{d\eta}$, $F_{d\xi}$) of η, ξ components.

2.3 Numerical algorithm method

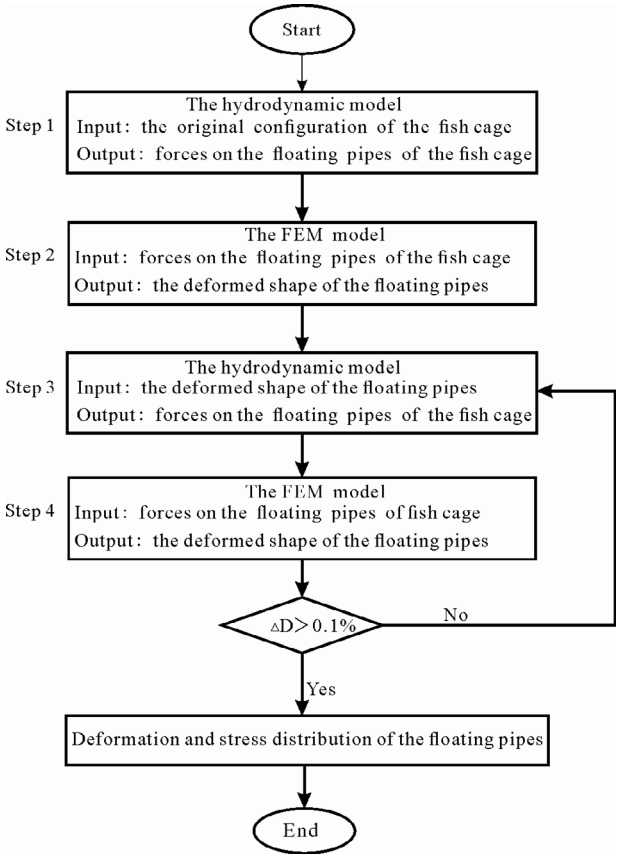

Fig. 4. Flow chart for joint use of the FEM model and the hydrodynamic model.

The numerical analysis was performed based on combination of the finite element model and the hydrodynamic force model. The term "iteration" is introduced to describe the calculation procedure. Iteration means using the finite element (FE) model and the hydrodynamic force model based on the Morison's equation and lumped-mass model to meet the precision requirement. Each repetition of the process is called an "iteration". The calculation procedure includes four steps: Step 1 is to simulate the fish cage without considering the deformations of nets and floating pipes. The drag force on the floating pipes

in the current using was calculated using the hydrodynamic force model. In Step 2, according to the floating pipes configuration, the FE model of the floating pipes was constructed using the shell element. The forces on the floating pipes obtained in the Step 1 are applied in the FE model. The deformed shape of the floating pipes can be obtained. In Step 3, the forces on the deformed floating pipes are calculated again using the hydrodynamic force model. In Step 4, the deformations of floating pipes are calculated. The terminal criterion of the calculation procedure is defined as $\Delta D = (Di+1- Di)/Di+1$, where Di+1 and Di are the diametric deflection of two adjacent calculations. If $\Delta D < 0.001$, it was determined that the force acting on the net structure is stable and the configuration of the floating pipes is the equilibrium position with fluid-structure interaction taken into account. Thus the calculation procedure is completed. Otherwise, continue with the next iteration of the procedure and repeat Steps 3 and 4 until the criterion meets the precision requirement. Finally, the deformations and stress distribution of the floating pipes can be obtained.

3 EXPERIMENTAL VERIFICATIONS

3.1 Validation 1 (the finite element model)

3.1.1 Laboratory setup

The circular ring experiments were conducted by Fredriksson et al.[7]. The laboratory experiment consisted of five individual pull tests performed on 3.66 meter diameter circular rings of HDPE pipe. The parameters of the circular pipe ring are provided in the Table 1. The rings were fixed at two locations on one side spaced approximately 2.8 meters apart along the arc. On the other side, a single rope with an inline load cell was attached to the ring. The test was repeated five times with different specimens.

Table 1 Parameter of the circular pipe

Parameter	Value
Diameter	3.66m
Pipe diameter	8.89cm
Wall thick ness	0.574cm
Yield stress	2.41×108 Pa
Poisson’s ratio	0.42
Modulus	6.67×108 Pa

3.1.2 Numerical simulation and comparison with the physical tests

Numerical simulations of the circular ring tests were performed using the finite element method. ANSYS/Standard was employed to perform numerical simulations. The finite element model was built using the geometric properties of the pipe same as the circular ring laboratory tests. The pipe is meshed using 6400 nodes and 6400 rectangular shell elements. The fixed and load boundary conditions were set in the same location as the laboratory tests.

The numerical and physical results of the circular ring are shown in Fig. 5. It can be seen that the pipes have same deformed shape. The wrinkle at the load point was observed from both simulation and physical tests. Additionally, the relationship of the rope force and the diametrical deflection is shown as Fig. 6. The results indicate that the numerical method makes it a suitable tool for analyzing deformation characteristics of the pipes.

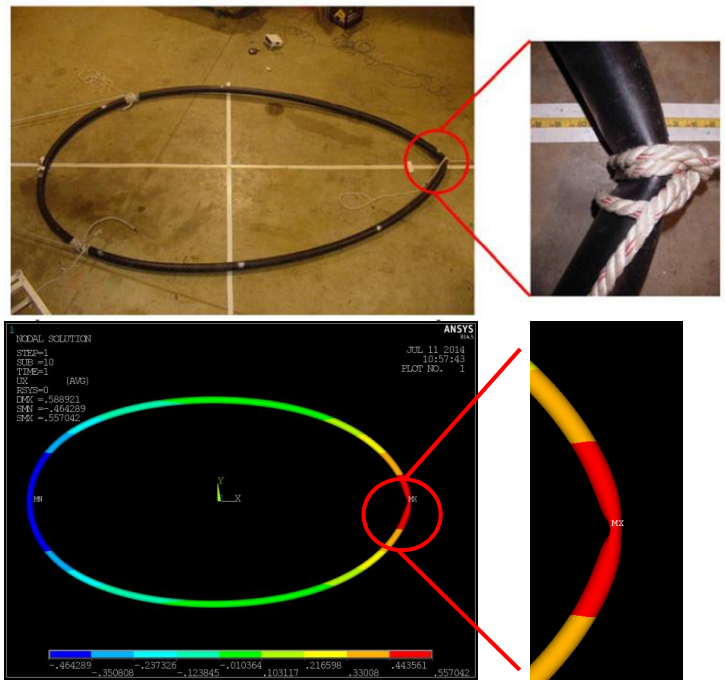

Fig. 5. Comparison the results between the physical test and numerical simulation.

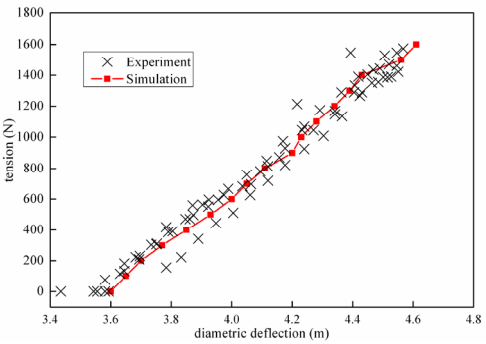

Fig. 6. Comparisons of the diametric deflection between the physical tests and numerical simulations.

3.2 Validation 2

3.2.1 Laboratory setup

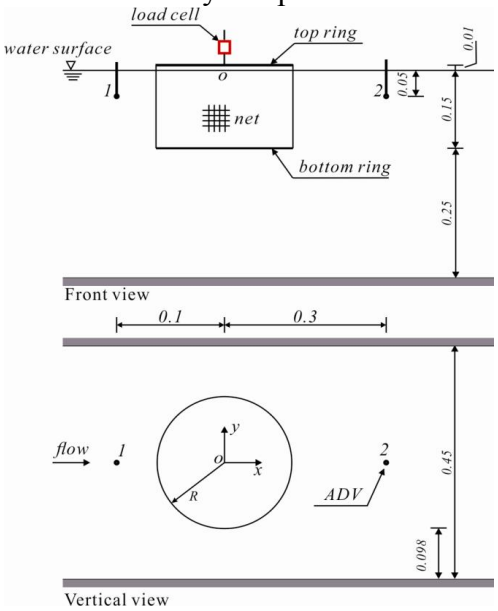

Fig. 7. Schematic diagram of the physical model and general setting of the measurement points(unit: m).

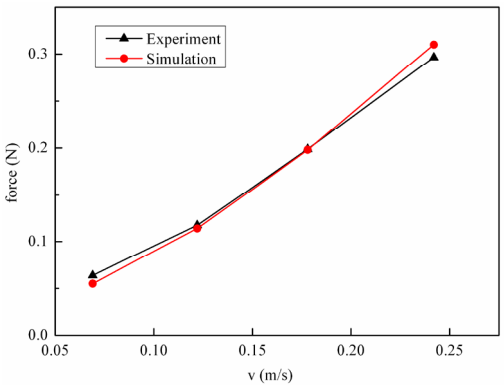

Fig. 8. Comparison of numerical and experimental net drag forces for different incoming velocities.

The physical model tests were conducted in a wave-current flume. As shown in Fig. 7, the physical model was installed in the centre of the flume. The net cage model consists of a top

ring, a cylindrical net and a bottom ring attached to the bottom of the net. The radius of the cylindrical net R is 0.127 m, and the depth is 0.16 m. The tested net is a knotted net with a 3 mm knot diameter and the mesh bar length was 20 mm. The top of the net is mounted on the top ring, which is fixed 1 cm above the free surface to avoid influencing the flow field (see Fig. 7). The bottom ring is suspended around the bottom opening of the cylindrical net as weight system and the weight mass is 8 g. Configuration of the flexible net was recorded using a charge coupled device (CCD) camera. In the physical model tests, 4 different incoming velocities cases are applied, 0.069, 0.122, 0.178 and 0.242 m/s. The water depth is equal to 0.4 m. Each test was repeated three times to assess the repeatability of the measurements.

3.2.2 Numerical simulation and comparison with the physical tests

The numerical simulation of a net cage in currents was performed using the lumped-mass model. The characteristics of the simulated net cage were the same as the tested net. The mesh-grouping method is used to reduce the number of the meshes of the net chamber. In the grouped model, the number of the meshes in the circumferential direction is 10, and it is 4 in the depth direction. Thus, four meshes were grouped into one mesh and the net chamber is divided into 40 plane-net elements.

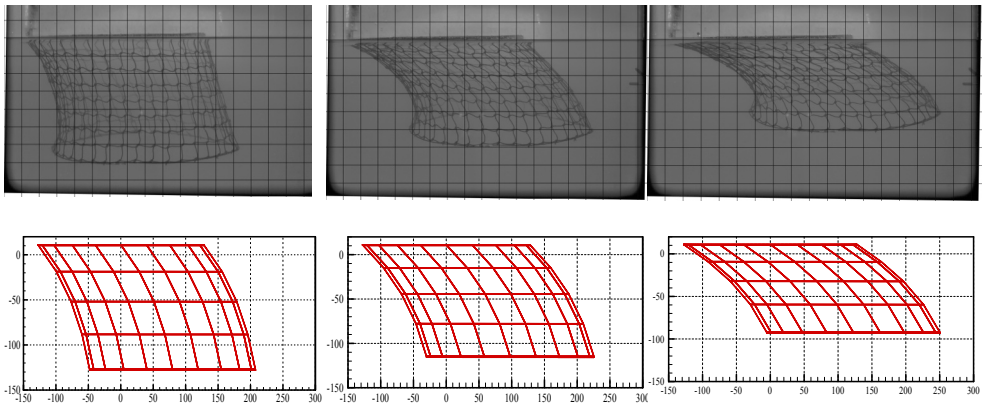

Fig. 9. Comparison of the deformation of a net cage between the numerical simulation and physical model test at different current velocities

The drag forces of the net cage were calculated at different incoming velocities and the numerical results compared with the experimental data are shown in Fig. 8. The numerical results are in accordance with the results of the experiment and the maximum relative error is 5%. The deformation of the net cage in currents is qualitatively described in Fig. 9. It can be observed that the deformation of the net cage increases obviously with increasing current velocity. Comparisons of the net deformation between the numerical simulations and the laboratory experiments present a satisfactory result.

4 NUMERICAL SIMULATIONS

4.1 Numerical simulation of the fish cage in different flow velocity

In this section, simulations of both an entire net cage at different flow velocity are performed based on dynamic analysis and finite element method to analysis the effect of the

net on the capability of the floating pipes. The geometric and material parameters of net cage designed according the real sea state is provided by Yellow Sea Fisheries Research Institute, Chinese Academy of Fishery Sciences, as shown in Table 3. Fig. 3(a) gives a sketch of fish cage system. The numerical simulations are performed with incoming velocity v=0.25, 0.5, 0.75, 1.0, 1.25, 1.5m/s.

Table 2 The geometric and material parameters of net cage.

Component	Parameter	Value
Floating pipe	General diameter	15.9 m
	Circumference	50 m
	Pipe diameter	0.25 m
	Density	953 kg/m3
	Elastic modulus	6.67×108 Pa
Net	Diameter	0.002 m
	Density	1140 kg/m3
	Height	8 m
Bottom ring	General diameter	15.9 m
	Diameter	0.6 m
	Linear massa	4 kg/m
Sinkers	Mass	300 kg

[a] the bottom ring is made of the HDPE pipe filled with iron sand

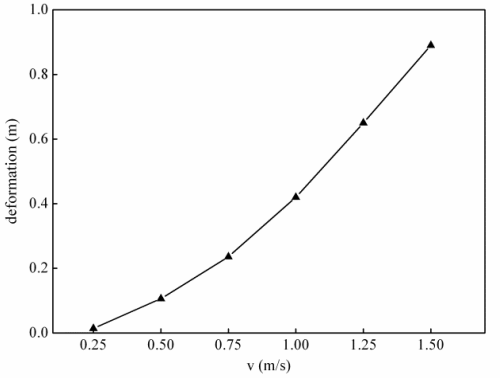

Fig. 10. The maximum deformations of the floating pipes.

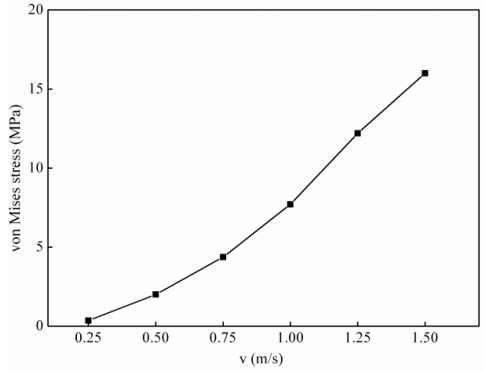

Fig. 11. The maximum von Mises stress of the floating pipes.

Fig. 10 and Fig. 11 show the maximum deformations and von Mises stress of the floating collars different flow velocity. The results show that the deformations and stress of the floating collars are much small and drastically increases with the increase of the velocity. Although the stress is less than yield strength (25 MPa), the high stress will reduce the fatigue life of the floating pipes. Therefore, it is crucial to fully take into account the influence of the velocity.

4.2 Effect of the mooring line arrangement on the stress distribution of the floating pipes

The effect of the mooring line arrangement of the fish cage is another factor that attracts the interest of fish farmers. Fig. 12 shows the schematic representation of the three different mooring arrangements. The parameters of the floating pipes are same as the Section 4.1 and the incoming velocity is 1.5 m/s.

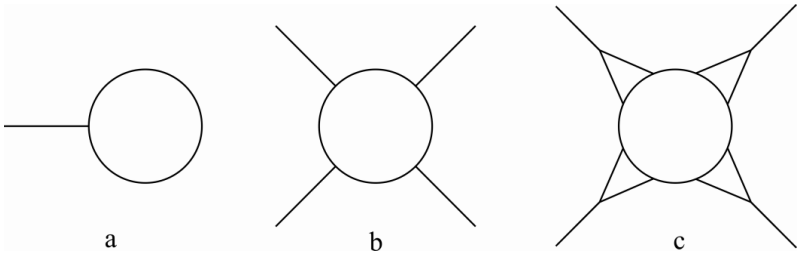

Fig. 12. The three different mooring line arrangements.

Fig. 13 shows the maximum stress of the floating pipes with different mooring line arrangements. With one attachment point, the maximum stress of the floating pipes is 16 MPa. When more mooring lines are used as shown Fig. 13(b) and Fig. 13(c), the maximum stress of the floating pipes are 6 MPa and 3 MPa, respectively. The maximum displacements of x-axis direction with the three mooring line arrangements are 0.867, 0.213 and 0.102m, respectively. It can be concluded that increasing the mooring line can effectively reduce stress levels and deformations of the floating pipes and therefore is advantageous to the safety of the fish cage. Additionally, it can be seen from the Fig. 13 that the high stress areas are usually observed near the mooring line attachment points. Therefore, those positions should be paid much attention in the structural design.

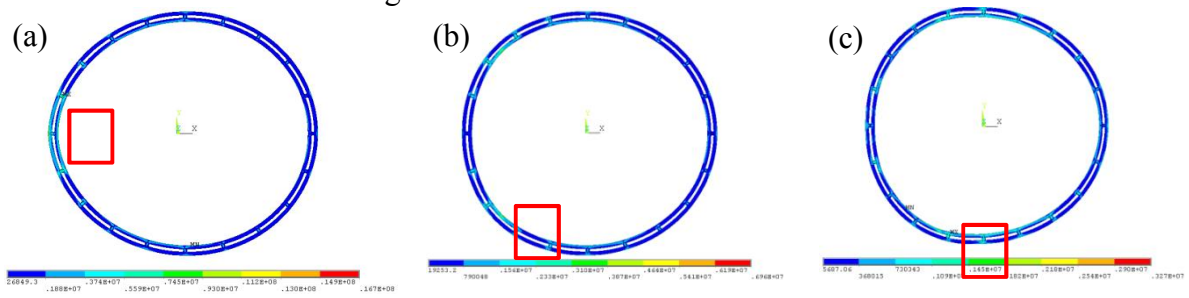

Fig. 13. The stress distribution of the floating pipes with different mooring line arrangement

4.3 The single point mooring cage system with multiple net cages

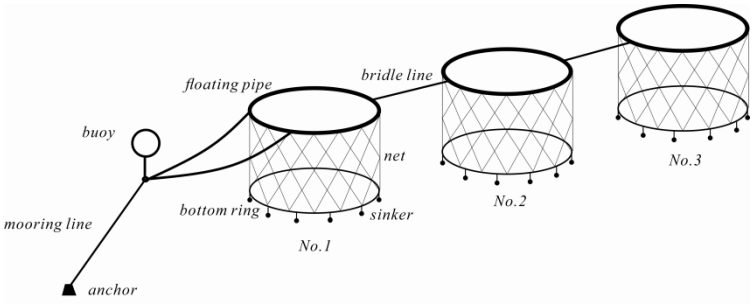

Fig. 14. The SPM cage system with three net cages.

The SPM system is widely used in aquaculture farm. Many researchers have conducted correlation studies on the hydrodynamic characteristic of the SPM cage systems (Decew et al.[8]; Huang and Pan[9]). In this section, simulations of the tripartite-cage system in currents are performed based on the hydrodynamic model and finite element method. Fig. 14 shows

the single point mooring cage system with three net cages. To discuss the difference of the tripartite-cage system, the net cages are numbered as shown in Fig. 14. As the net cages are arranged in a row, the shielding effect on the rear net cage should be considered. Based on the previous research (Loland, G.[10]), a reduction factor of 0.85 is adopted in the numerical simulation to represent the retardation effect on the water particle speed after passing through each previous net.

Table 3 The maximum stress and deformations of the floating pipes.

	Maximum deformations	Maximum stress
No.1	3.91 m	25 MPa
No.2	4.67 m	25 MPa
No.3	0.75 m	14 MPa

Table 5 shows the maximum stress and deformations of floating pipes of each cage. For the tripartite-cage system, the maximum stress of the No. 3 cage is lower than the yield stress. While the numerical results show that the maximum stress of the No. 1 and 2 cages reaches the yield stress. Fig.15 shows the stress contours of the deformed pipes of the two cages. As shown in the Fig, 16, the stress level of the No. 2 cage is higher than that of the No. 1 cage and the yield-region of the No. 2 cage is much greater than that of the No. 1 cage. Additionally, because of the drag of the front and rear cages, the deformations of *x*-axis direction of the No. 2 cage has drastically increased. It can be concluded that the middle cage is the most dangerous cage for the tripartite-cage system.

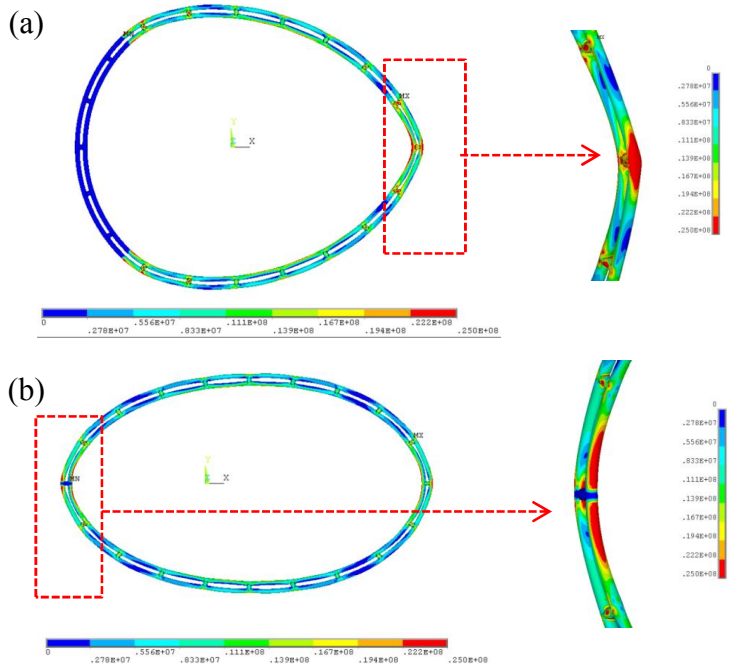

Fig. 15. The stress contours of the deformed pipes of (a) the No. 1 cage and (b) the No. 2 cage

5 CONCLUSIONS

A numerical model based on joint use of the finite-element method and the hydrodynamic model was presented in current study. Combining the two proposed model, the stress distribution and maximum stress of the floating pipes were calculated. On that basis, the simulations of floating pipes under high speed water flow were performed to investigate the deformations and the stress distribution. The simulations results show that the stress of the floating pipes dramatically increases with the flow velocity increasing. Comparing results of floating pipes with different mooring line arrangements indicates that increasing mooring lines can efficiently lower the stress of the floating pipes. The simulation of the SPM cage system with multiple net cages in currents was performed and the results show the middle cage is most dangerous.

REFERENCES

[1] Tsukrov, I., Eroshkin, O., Fredriksson, D.W., Robinson, S.M., and Celikkol, B., 2003. *Finite element modeling of net panels using a consistent net element*. Ocean Engineering 30(2), 251-270.

[2] Lader, P.F., Enerhaug, B., 2005. *Experimental investigation of forces and geometry of a net cage in uniform flow*. IEEE Journal of Oceanic Engineering 30 (1), 79-84.

[3] Moe, H., Fredheim, A., Hopperstad, O.S., 2010. *Structural analysis of aquaculture net cages in current*. Journal of Fluids and Structures 26, 503-516.

[4] Kristiansen, T., Faltinsen, O.M., 2012. *Modelling of current loads on aquaculture net cages*. Journal of Fluids and Structures 34, 218-235.

[5] Zhao, Y.P., Bai, X.D., Dong, G.H., Bi, C.W., Gui, F.K., 2014. *Numercial analysis of the elastic response of a floating collar in waves*. Ocean Engineering 95, 175-182.

[6] Brebbia, C.A., Walker, S., 1979. *Dynamic Analysis of offshore Structures*. Newnes-Butterworths, London, UK, pp. 109-143.

[7] Fredriksson, D.W., DeCew, J.C., Tsukrov, I., 2007. *Development of structural modeling techniques for evaluating HDPE plastic net pen used in marine aquaculture*. Ocean Engineering 34(16), 2114-2137.

[8] Decew, J., Tsukrov, I., Risso, A., Swift, M.R., Celikkol, B., 2010. *Modeling of dynamic behavior of a single-point moored submersible fish cage under currents*. Aquacultural Engineering 3(2), 38-45.

[9] Huang, C.C., Pan, J.Y., 2010. *Mooring line fatigue: A risk analysis for an SPM cage system*. Aquacultural Engineering 42(1), 8-16.

[10] Loland, G., 1991. *Current forces on and flow through fish farms*. Ph.D. Dissertation. Institute of Technology, Trondheim, Norway.